

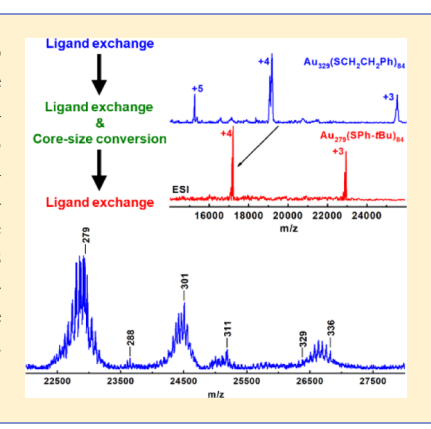
Core Size Conversion of Au₃₂₉(SCH₂CH₂Ph)₈₄ to Au₂₇₉(SPh-tBu)₈₄ **Nanomolecules**

Senthil Kumar Eswaramoorthy, Naga Arjun Sakthivel, and Amala Dass*

Department of Chemistry and Biochemistry, University of Mississippi, Oxford, Mississippi 38677, United States

Supporting Information

ABSTRACT: We report the core size conversion of Au₃₂₉(SCH₂CH₂Ph)₈₄ to Au₂₇₉(SPh-tBu)₈₄ plasmonic nanomolecules. The mass spectrometric studies have revealed an unprecedented reaction pathway for the Au₃₂₉ to Au₂₇₉ core size conversion reaction via three steps. First, ligand exchange with 4-tert-butylbenzenethiolate occurs, followed by simultaneous progression of ligand exchange and core-size conversion with the loss of one Au atom after another and finally reaching completion with full ligand exchange on Au₂₇₀. Typically, when a core size conversion occurs in molecule-like nanomolecules, different sizes have different electronic and structural properties; in this case, both the reactant and the product possess plasmonic behavior and bulk-like facecentered cubic structures. Also, this is the first report to study the core size transformation involving a difference of 50 metal atoms but identical 84 ligand count.



INTRODUCTION

The synthesis of thiolate-protected stable molecules of gold with molecular and metallic properties is highly pursued for various practical applications. 1-4 These molecules of gold, also known as gold nanomolecules (AuNMs), can be synthesized via bottom-up, direct synthetic protocols followed by postsynthetic treatment or top-down approach involving core size conversion of one stable AuNM to another.2 The direct synthesis of AuNMs results in a polydisperse product, which produces a mixture of stable sizes upon thermochemical treatment (or etching), requiring purification to obtain pure AuNMs.5 Ligand exchange or place exchange reactions on NMs have been shown to functionalize NMs with new ligand shell or to make new sizes via core size conversion and tune the properties.⁶⁻²⁰ The core size conversion is dictated by the ligand being employed in the reaction, and each ligand has a unique series of discrete stable sizes with distinct structure and property.2,21

Highly pure samples are desired for various structural and property studies and application development. Core size conversion of AuNMs by ligand exchange with different ligands has proven to be a unique way to make pure AuNMs exclusively in high yields. ^{2,22,23} It has been shown to circumvent the need for demanding purification processes in obtaining pure AuNMs in high yields, for example, Au₃₀, Au₃₆, and Au₁₃₃. Recently, etching of a crude with different types of ligands (aliphatic, aromatic, and bulky) has been shown to produce pure, stable AuNMs. Etching of crude differs from core size transformation where the etching ligands employed in the sequential process are of same class that supports the AuNMs size of interest without inducing core size conversion, however, destabilizes other metastable sizes in the process yielding the desired AuNMs in high purity. For

example, pure Au₃₆ has been obtained in high yield by sequential etching of a polydisperse phenylethanethiolateprotected gold nanocluster crude mixture with thiophenol and then with 4-tert-butylbenzenethiol (TBBT). 25

Significant progress has been made toward understanding the transformational and controlled ligand exchange chemistry in AuNMs with Au <50 atoms. 2,11,12,28-41 Transformation from one stable size to another provides access to an entirely new set of properties than the precursor AuNMs, whereas controlled ligand exchange retains the core structure but tunes the electronic property. 2,42 For example, Au₃₈(SC₂H₄Ph)₂₄ with thiophenol forms Au₃₆ and Au₃₈ under thermodynamic and kinetically controlled reactions, respectively. 43 The thermodynamic product (Au₃₆) has entirely different atomic and electronic structures with higher band gap than the precursor, whereas the kinetic product⁴³ (Au₃₈) has similar atomic structure and optical features. In some cases, interconversion between two stable sizes has been observed as well.^{24,44} Recently, new branches of core conversion reactions such as oxidation-induced core size conversion, 45 fusion reaction without any coreactants, 46 and seed-mediated growth⁴⁷ have been demonstrated.

To date, only little information is known on the transformational chemistry of AuNMs with Au >~100 atoms and plasmonic nanocrystals. Au₉₉, Au₁₀₂, Au₁₀₃, and Au₁₃₃ are the four larger AuNMs that have been synthesized via core conversion method. ^{26,27,48–50} On the plasmonic nanocrystal regime, crystal structure, optical and catalytic properties of the smallest thiolate-protected metallic gold nanocrystal, Faradaurate $\mathrm{Au}_{279}(\mathrm{TBBT})_{84}$ has been recently reported. $^{4,51-53}$ Au_{279}

Received: February 28, 2019 Published: March 28, 2019

9634

has been obtained by direct synthesis⁴ and etching⁵² of a polydisperse phenylethanethiolate-protected gold nanocluster crude mixture with phenylethanethiol (SPC₂) followed by 4tert-butylbenzylthiol and core conversion with TBBT.

The phenylethane- and aliphatic thiolate-protected AuNM series have been studied over two decades, but these aliphatic systems are difficult to crystallize. 1,54,55 Recently, the crystal structure of the widely studied aliphatic thiolate-protected Au₁₄₄ has been crystallized two decades after its discovery, and it was similar to the icosahedral structure predicted by theoretical computations. 56-58 The introduction of rigid and bulky thiolated ligands such as TBBT favors the single-crystal growth. 59,60 TBBT-protected AuNM series are widely studied in recent years, and all of the sizes in the TBBT series have been crystallographically resolved.²¹ Au₂₇₉ is the largest crystal structure of thiolate-protected AuNMs reported to date.4 The highly stable, benchmark molecule-like AuNMs in aliphatic thiolate series core-convert to stable sizes in TBBT series upon ligand exchange with TBBT (Au₂₅ to Au₂₈, Au₃₈ to Au₃₆, and Au₁₄₄ to Au₁₃₃). ^{23,61,62} However, the core size conversion on the plasmonic regime has not been studied in detail. In this work, we have investigated the core size conversion reaction of Au₃₂₉(SC₂H₄Ph)₈₄, the next stable size in aliphatic thiolateprotected series of AuNMs^{3,63} to Au₂₇₉(TBBT)₈₄ by electrospray ionization (ESI), matrix-assisted laser desorption ionization (MALDI) mass spectrometry, and absorption spectroscopy to shed light on how the core conversion reaction progresses in plasmonic nanocrystals. A closely related composition for the 76.3 kDa has been reported as $Au_{333}(SC_2H_4Ph)_{79}$, and few other studies have used the same composition as well. ^{55,64,65} However, a detailed study on the composition of 76.3 kDa species with various ligands has revealed the molecular formula 63 to be Au₃₂₉(SC₂H₄Ph)₈₄, and the validity of Au₃₃₃(SC₂H₄Ph)₇₉ composition remains to be

The crystal structure of Au₂₇₉ revealed that it has a bulk-like face-centered cubic (fcc) atomic structure. Au₂₇₉ has a Au₂₄₉ metal core made of truncated octahedral core (Au₂₀₁) with four concentric shells and a 48 atom ad-layer on the {111} facets of Au₂₀₁ protected by a ligand shell with 30 gold atoms and 84 ligands. The powder X-ray diffraction, atomic pair distribution function, and electron microscopy have revealed that the Au₃₂₉ also has an fcc atomic structure.⁶⁶ However, it remains to be crystallographically studied. It is worth noting that the change in the incoming ligand leads to two different combinations with 50 gold atoms difference (329 and 279) but same number of ligands. 4,66

Figure 1 reveals the reaction progress monitored by MALDImass spectra (MS), where Au₃₂₉ (starting material) is converted into Au₂₇₉ after reacting with TBBT at 80 °C for 6 days. The multiple charged peaks observed in MALDI-MS are lower in mass than the molecular ion peak mass because of fragmentation under the laser beam. The pure Au₃₂₉ was obtained as detailed in the Experimental Section. The MALDI-MS of Au₃₂₉ reveals the 1+ and 2+ peaks at \sim 73 and \sim 36.5 kDa, respectively (Figure 1). After 2 days of reaction, two new peaks were observed at ~64.5 and ~32.5 kDa corresponding to 1+ and 2+ charge states of Au₂₇₉, respectively, indicating the onset of Au₃₂₉ to Au₂₇₉ core size conversion. Also, the peak maxima of Au₃₂₉ have moved from ~73 to ~70 kDa intermediate species (see below ESI data of the 2 days sample) because of the core size conversion. The four-day sample shows that the ~64.5 kDa peak is prominent and ~70

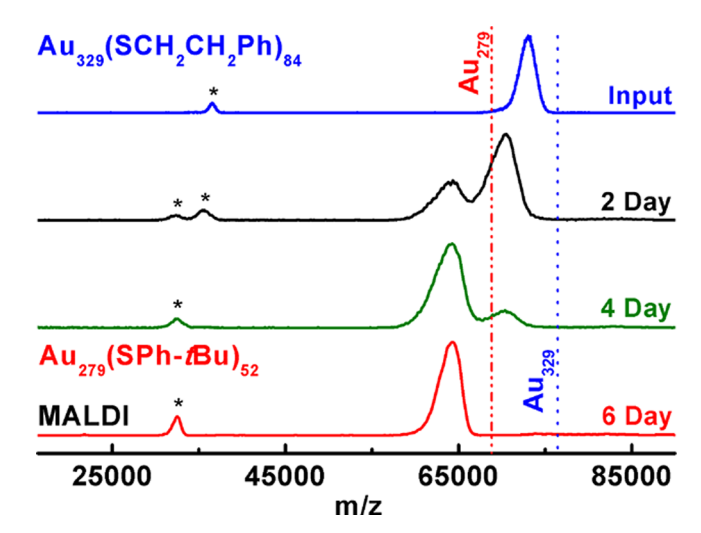


Figure 1. MALDI MS of the starting material Au₃₂₉(SCH₂CH₂Ph)₈₄ and its transformation to Au₂₇₉(SPh-tBu)₈₄ on reacting with TBBT at 80 °C over 6 days. The dot and dash-dot-dot vertical lines correspond to the molecular mass of Au₃₂₉ and Au₂₇₉, respectively. * indicates the 2+ charge state of respective nanomolecules.

kDa peak intensity has decreased as the reaction proceeds (Figure 1). The complete core size conversion to Au₂₇₉ was observed after 6 days of reaction with only (1+ and 2+) peaks corresponding to Au₂₇₉ that were observed in the MS (Figure

ESI-MS was employed to further study the core size conversion reaction in detail. Figure 2 shows the ESI-MS of the

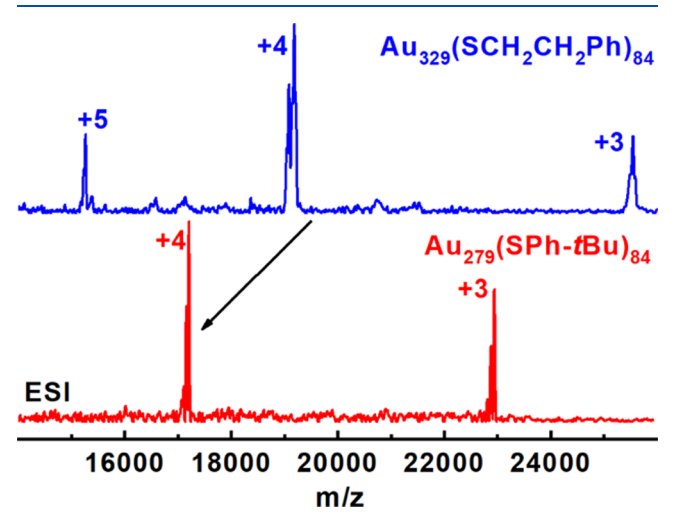


Figure 2. ESI-MS of Au₃₂₉(SCH₂CH₂Ph)₈₄ transforming to Au₂₇₉(SPh-tBu)₈₄ upon reacting with TBBT at 80 °C for 6 days.

starting material (Au₃₂₉) and the final product (Au₂₇₉). Au₃₂₉(SC₂H₄Ph)₈₄ has a molecular weight of 76 329 Da, and it was observed in 3+, 4+, and 5+ charge state peaks at 25 546 Da (3 Cs adducts), 19 182 Da (3 Cs adducts), and 15 267 Da, respectively (Figure 2). The final product, Au₂₇₉(SPh-tBu)₈₄, has a molecular weight of 68 836 Da, and it ionized in 3+ and 4+ charge states with peaks at 22 944 Da and 17 208 Da, respectively. The core size conversion reaction was completed after 6 days and as evidenced by the ESI-MS.

The Au₃₂₉(SPC₂)₈₄ to Au₂₇₉(TBBT)₈₄ reaction proceeds in three stages, first ligand exchange with TBBT occurs followed The Journal of Physical Chemistry C

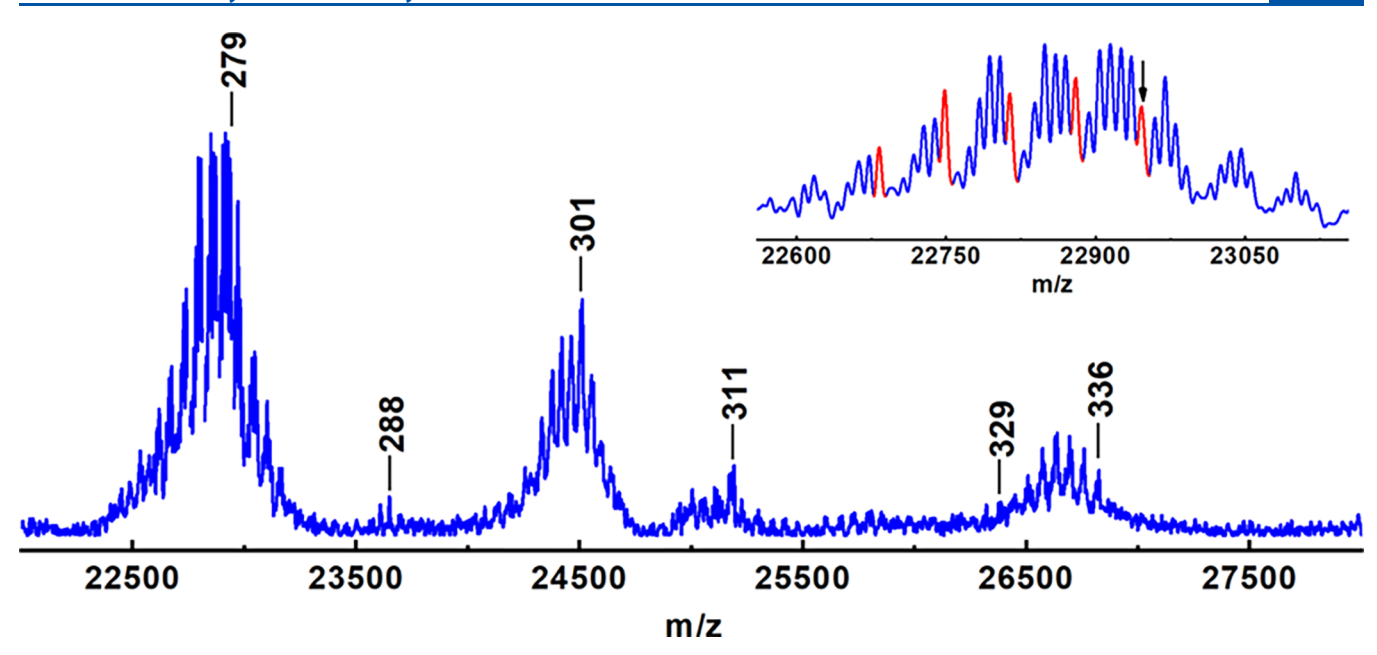


Figure 3. ESI-MS of a 3+ peak in two-day reaction sample showing the occurrence of ligand exchange and core size conversion simultaneously. The peak assignment of 288, 301, 311, 329, and 336 Au atoms has 84 TBBT ligands and $3Cs^+$ adducts with it. The inset is in 22.5–23.1 kDa range to reveal the Au_{279} formation (indicated by a red peak with an arrow). The full spectrum is provided in Figure S1.

by simultaneous core size conversion and ligand exchange reaction, and finally reaction reaches completion with complete ligand exchange by TBBT ligands. Figure 3 reveals the ESI-MS data of the 3+ charge state in 22-28 kDa m/z range for a twoday reaction sample. Intriguingly, the thiolate ligands on the monolayer count remain 84 throughout. It is worth noting that mass spectrometry of larger nanomolecules is difficult and as the ligand exchange and/or core size conversion reactions are performed on large nanomolecules, analyzing that the reaction progress becomes increasingly difficult. The mass difference between PC₂S (137.22 Da) and TBBT ligands (165.27 Da) is 28.06 Da. Therefore, a 3+ charge state peak corresponding to the ligand exchange reaction would have an envelope of peaks with a mass difference of 9.3 Da. Additionally, changes in the number of gold atoms during core size conversion and varying Cs⁺ adduct formation pose the major challenge in analyzing the data. The compositions for the intermediate samples were assigned based on the multiple charge state peaks, and in some cases, there are close overlap between two possible combinations and the probable assignments have been included in this report. For example, [Cs₃]³⁺ has a mass of 132.91 Da and two Au atoms have a closer mass of 131.31 Da, where $\sim \pm 1-2$ Da falls in the range of experimental mass error possible for larger nanomolecules.

Figure 3 reports the ESI-MS data for the two-day sample in the 3+ charge state region of 22–28 kDa, and the inset shows the 22.5–23.1 kDa range to reveal the core size conversion and ligand exchange reaction proceeding simultaneously. First, Au₃₂₉(PC₂S)₈₄ undergoes ligand exchange to form Au₃₂₉(TBBT)₈₄ with few unexchanged PC₂S ligands. The Au₃₂₉(TBBT)₈₄ composition is metastable, and the reaction proceeds to core conversion phase, leading to another metastable size after well-known (329,84) composition up to Au₃₃₆(TBBT)₈₄ with increments of one Au atom, that is, 329, 330, 331, ..., 336 (Figure 3). MALDI-MS data for two-day sample (Figure 1) also corroborate the formation of Au₂₇₉ core, and the figure inset shows envelope of peaks and the fully exchanged Au₂₇₉(TBBT)₈₄³⁺ at 22 945 Da (red peak indicated

by an arrow). The inset has about 8 envelopes of peaks, and their m/z values are listed in Table S1. The peaks indicated in red to the left of $\mathrm{Au_{279}(TBBT)_{84}}^{3+}$ have a m/z difference of 66 Da corresponding to one Au atom, and their compositions are $\mathrm{Au_{278}(TBBT)_{84}}^{3+}$, $\mathrm{Au_{277}(TBBT)_{84}}^{3+}$, $\mathrm{Au_{276}(TBBT)_{84}}^{3+}$, and $\mathrm{Au_{275}(TBBT)_{84}}^{3+}$. The envelope of blue peaks adjacent to red peaks corresponds to unexchanged PC₂S ligands with \sim 9 Da difference.

Finally, the core size conversion to stable $Au_{279}(TBBT)_{84}$ occurs (Figure 4). After 4 days of reaction, only fewer unexchanged PC_2S ligands are observed near the molecular peak (Figure 4, olive spectra). The $Au_{279}(TBBT)_{84}$ then resolves to be the prominent stable compound, and $Au_{278}(TBBT)_{84}^{3+}$ and $Au_{277}(TBBT)_{84}^{3+}$ peaks were also observed but not as significant as 2–4 day samples. The Au_{278} , Au_{277} , and Au_{276} are kinetic products which are stable for a certain period, and eventually, they converge toward Au_{279} as the reaction progresses. Similar phenomena with one Au atom difference during core size conversion of larger nanomolecules have been observed as a kinetic product in the transformation of Au_{144} to Au_{133} where $Au_{132}(TBBT)_{52}$ was present during intermediate samples and goes down in intensity with time and negligible toward the end. 26

The molecule-like (Au₃₈ to Au₃₆) nanomolecular core size conversion involves striking changes in optical properties between the starting material and product.² Absorption spectroscopy was performed to study how the optical property of plasmonic nanomolecules would be affected by the core size conversion reaction. The optical property of the starting material (Au₃₂₉) and the product (Au₂₇₉) is compared in Figure 5. The blue curve in Figure 5 corresponds to Au₃₂₉. The UV–vis absorption spectra of Au₃₂₉ have a plasmonic band centered ~495 nm, and upon transformation to Au₂₇₉ by reacting with TBBT, the product also exhibits a SPR band; however, it is red shifted to ~510 nm. It is worth noting that despite the loss of 50 Au atoms, the molecule is still plasmonic and the manifestation of SPR on 279 has been attributed to the presence of phenyl rings.⁵¹

The Journal of Physical Chemistry C

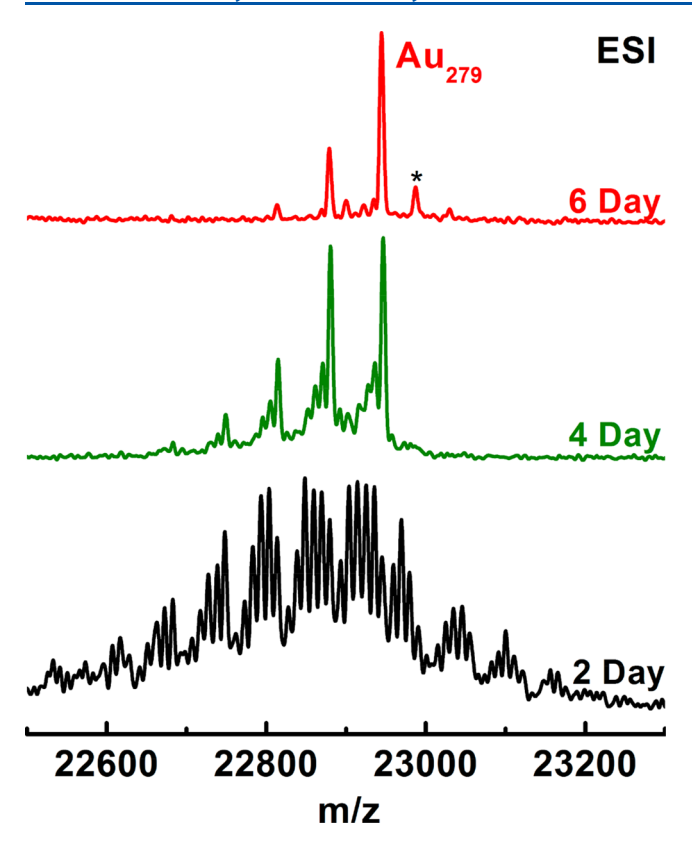


Figure 4. ESI MS (zoom in) of the intermediates showing the ligand exchange and conversion.

In summary, we have studied the core size conversion of Au₃₂₉ to Au₂₇₉ by using MALDI and ESI mass spectrometry and absorption spectroscopy. The core size conversion takes place in three steps, first ligand exchange, then ligand exchange and core size conversion occur simultaneously, and finally reaction reaches completion with complete ligand exchange by exogenous ligands. The mass spectrometric results have revealed the unprecedented reaction pathway involving ligand exchange and core size conversion with loss of one gold atom after another, retaining a constant 84 ligand monolayer count. The optical absorption studies have shown that both the starting material and the product are plasmonic as reported.⁵¹

EXPERIMENTAL SECTION

Materials. Hydrogen tetrachloroaurate(III) (HAuCl₄· $3H_2O$), sodium borohydride (NaBH₄, 99%), tetraoctylammonium bromide (TOABr), TBBT (TCI, 99%), phenylethylmercaptan (Sigma-Aldrich), cesium acetate (Acros, 99%), anhydrous ethyl alcohol (Acros, 99.5%), and *trans*-2-[3[(4-tertbutyl-phenyl)-2-methyl-2-propenylidene]malononitrile (DCTB matrix) (Fluka, ≥99%) were used. High-performance liquid chromatography grade solvents such as tetrahydrofuran, toluene, methanol, and butylated hydroxytoluene-stabilized tetrahydrofuran were obtained from Fisher Scientific. All of the materials were used as received.

Synthesis. The core conversion of $Au_{329}(SCH_2CH_2Ph)_{84}$ to $Au_{279}(SPh\text{-}tBu)_{84}$ was performed in two primary steps, namely, Au_{329} synthesis and core conversion of Au_{329} to Au_{279} . First, $Au_{329}(SCH_2CH_2Ph)_{84}$ was synthesized by slightly modifying the previously reported method. 66 $Au_{329}(SCH_2CH_2Ph)_{84}$ preparation was carried out in three steps. First, crude nanoparticles were synthesized which

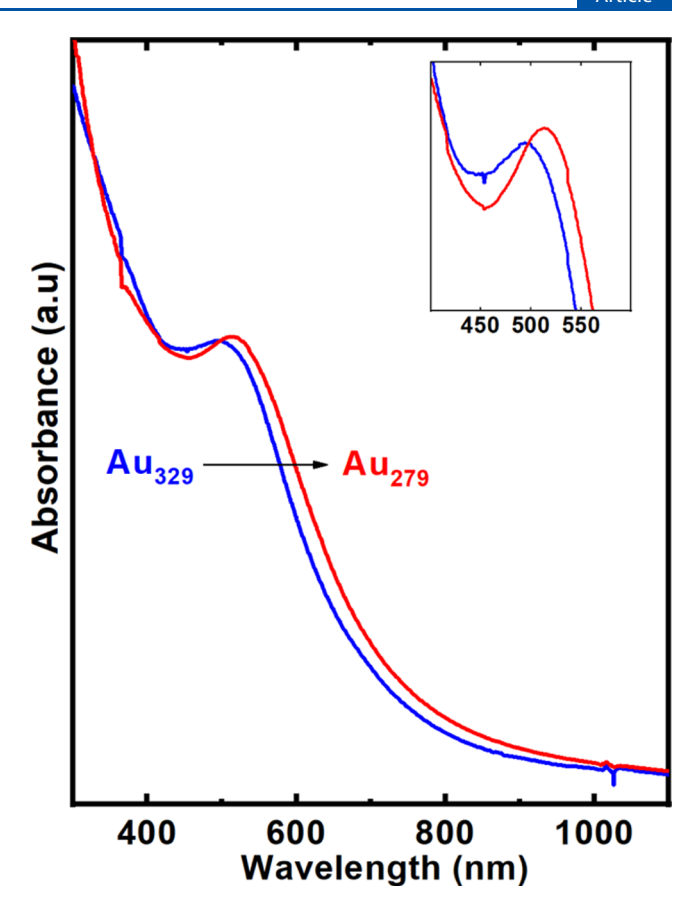


Figure 5. UV—vis absorption spectra of $Au_{279}(SPh\text{-}tBu)_{84}$ nanomolecules in comparison with the starting material $Au_{329}(SCH_2CH_2Ph)_{84}$ in toluene.

contain polydisperse gold nanoparticles with metastable sizes. Then, thermochemical treatment was done on the crude to narrow down the size and to remove the metastable clusters. Then, $Au_{329}(SCH_2CH_2Ph)_{84}$ was isolated using size-exclusion chromatography. Finally, $Au_{329}(SCH_2CH_2Ph)_{84}$ was subjected to ligand exchange with TBBT, and it undergoes core size conversion to form $Au_{279}(SPh-tBu)_{84}$.

Step 1: Au₃₂₉ synthesis. HAuCl₄·3H₂O (0.1 g) was dissolved in distilled water (10 mL), and TOABr (0.15 g) was dissolved in toluene (10 mL) separately. They were mixed together in a 100 mL round bottom flask under stirring (500 rpm). The mixture was stirred for 30 min. The organic layer was separated and placed in an ice bath for 30 min. Then, 70 µL of phenylethanethiol (Au/thiol = 1:2) was added, and the reaction was allowed for 1 h. The reaction mixture was then reduced by rapidly adding 0.1 g of NaBH₄ (Au/NaBH₄ = 1:10) dissolved in 5 mL of ice cold water. The solution changes to black color, indicating the formation of nanoparticles. The stirring was continued for about 24 h. The organic phase was then separated and rotary evaporated to remove the solvent. The crude product was washed with methanol and water mixture (3-4 times) to remove excess thiol and byproducts. The crude product was dissolved in toluene and etched with excess phenylethanethiol (60 mg of crude, 0.5 mL of toluene, and 0.5 mL of thiol) for ~3 days at 80 °C. Then, the etched product was rotary evaporated to remove the solvent and washed with methanol to remove excess thiol. Finally, Au₃₂₉(SCH₂CH₂Ph)₈₄ was isolated by size-exclusion chromatography.

Step 2: In this step, Au₃₂₉(SCH₂CH₂Ph)₈₄ was subjected to ligand exchange with *tert*-butylbenzenethiol for 6 days at 80 °C. The transformation of Au₃₂₉(SCH₂CH₂Ph)₈₄ to Au₂₇₉(SPh-tBu)₈₄ was monitored by MALDI and ESI mass spectrometry.

Instrumentation. The MALDI spectra were acquired from a Voyager DE PRO MALDI-time-of-flight (TOF)-MS instrument with the DCTB matrix. ESI MS were collected from Waters SYNAPT Q-TOF HDMS with tetrahydrofuran as the solvent. Baseline correction for Au₃₂₉ ESI-MS spectra was done by polynomial fitting (Figure 2). The cesium acetate was used to facilitate the ionization of nanomolecules with multiple charge states. The UV-vis absorption spectra were measured using a Shimadzu UV-1601 spectrophotometer.

ASSOCIATED CONTENT

S Supporting Information

The Supporting Information is available free of charge on the ACS Publications website at DOI: 10.1021/acs.jpcc.9b01953.

ESI-MS spectra and peak mass table (PDF)

AUTHOR INFORMATION

Corresponding Author

*E-mail: amal@olemiss.edu.

ORCID ®

Senthil Kumar Eswaramoorthy: 0000-0001-8015-1391

Naga Arjun Sakthivel: 0000-0001-8134-905X

Amala Dass: 0000-0001-6942-5451

Notes

The authors declare no competing financial interest.

ACKNOWLEDGMENTS

NSF-CHE-1808138 and NSF 1255519 supported the work performed by S.K.E., N.A.S., and A.D.

REFERENCES

- (1) Whetten, R. L.; Khoury, J. T.; Alvarez, M. M.; Murthy, S.; Vezmar, I.; Wang, Z. L.; Stephens, P. W.; Cleveland, C. L.; Luedtke, W. D.; Landman, U. Nanocrystal gold molecules. *Adv. Mater.* **1996**, *8*, 428–433.
- (2) Rambukwella, M.; Sakthivel, N. A.; Delcamp, J. H.; Sementa, L.; Fortunelli, A.; Dass, A. Ligand Structure Determines Nanoparticles' Atomic Structure, Metal-Ligand Interface and Properties. *Front. Chem.* **2018**, *6*, 330.
- (3) Dass, A. Faradaurate Nanomolecules: A Superstable Plasmonic 76.3 kDa Cluster. J. Am. Chem. Soc. 2011, 133, 19259–19261.
- (4) Sakthivel, N. A.; Theivendran, S.; Ganeshraj, V.; Oliver, A. G.; Dass, A. Crystal Structure of Faradaurate-279: Au₂₇₉(SPh-tBu)₈₄ Plasmonic Nanocrystal Molecules. *J. Am. Chem. Soc.* **2017**, *139*, 15450–15459.
- (5) Schaaff, T. G.; Whetten, R. L. Controlled Etching of Au:SR Cluster Compounds. J. Phys. Chem. B 1999, 103, 9394–9396.
- (6) Hostetler, M. J.; Green, S. J.; Stokes, J. J.; Murray, R. W. Monolayers in Three Dimensions: Synthesis and Electrochemistry of ω-Functionalized Alkanethiolate-Stabilized Gold Cluster Compounds. J. Am. Chem. Soc. 1996, 118, 4212–4213.
- (7) Heinecke, C. L.; Ni, T. W.; Malola, S.; Mäkinen, V.; Wong, O. A.; Häkkinen, H.; Ackerson, C. J. Structural and Theoretical Basis for Ligand Exchange on Thiolate Monolayer Protected Gold Nanoclusters. J. Am. Chem. Soc. 2012, 134, 13316–13322.
- (8) Guo, R.; Song, Y.; Wang, G.; Murray, R. W. Does Core Size Matter in the Kinetics of Ligand Exchanges of Monolayer-Protected Au Clusters? *J. Am. Chem. Soc.* **2005**, 127, 2752–2757.

- (9) Si, S.; Gautier, C.; Boudon, J.; Taras, R.; Gladiali, S.; Bürgi, T. Ligand Exchange on Au₂₅ Cluster with Chiral Thiols. *J. Phys. Chem. C* **2009**, *113*, 12966–12969.
- (10) Ni, T. W.; Tofanelli, M. A.; Phillips, B. D.; Ackerson, C. J. Structural Basis for Ligand Exchange on $Au_{25}(SR)_{18}$. *Inorg. Chem.* **2014**, 53, 6500–6502.
- (11) Huang, Z.; Ishida, Y.; Narita, K.; Yonezawa, T. Kinetics of Cationic-Ligand-Exchange Reactions in Au₂₅ Nanoclusters. *J. Phys. Chem. C* 2018, 122, 18142–18150.
- (12) Niihori, Y.; Hossain, S.; Kumar, B.; Nair, L. V.; Kurashige, W.; Negishi, Y. Perspective: Exchange Reactions in Thiolate-Protected Metal Clusters. *Apl. Mater.* **2017**, *5*, 053201.
- (13) Zheng, K.; Setyawati, M. I.; Leong, D. T.; Xie, J. Surface Ligand Chemistry of Gold Nanoclusters Determines Their Antimicrobial Ability. *Chem. Mater.* **2018**, *30*, 2800–2808.
- (14) Bootharaju, M. S.; Kozlov, S. M.; Cao, Z.; Shkurenko, A.; El-Zohry, A. M.; Mohammed, O. F.; Eddaoudi, M.; Bakr, O. M.; Cavallo, L.; Basset, J.-M. Tailoring the Crystal Structure of Nanoclusters Unveiled High Photoluminescence via Ion Pairing. *Chem. Mater.* **2018**, *30*, 2719–2725.
- (15) Nguyen, T.-A. D.; Jones, Z. R.; Leto, D. F.; Wu, G.; Scott, S. L.; Hayton, T. W. Ligand-Exchange-Induced Growth of an Atomically Precise Cu₂₉ Nanocluster from a Smaller Cluster. *Chem. Mater.* **2016**, 28, 8385–8390.
- (16) Song, Y.; Murray, R. W. Dynamics and Extent of Ligand Exchange Depend on Electronic Charge of Metal Nanoparticles. *J. Am. Chem. Soc.* **2002**, *124*, 7096–7102.
- (17) Hossain, S.; Kurashige, W.; Wakayama, S.; Kumar, B.; Nair, L. V.; Niihori, Y.; Negishi, Y. Ligand Exchange Reactions in Thiolate-Protected Au₂₅ Nanoclusters with Selenolates or Tellurolates: Preferential Exchange Sites and Effects on Electronic Structure. *J. Phys. Chem. C* **2016**, *120*, 25861–25869.
- (18) Tlahuice-Flores, A. Ligand Effects on the Optical and Chiroptical Properties of the Thiolated Au₁₈ Cluster. *Phys. Chem. Chem. Phys.* **2016**, *18*, 27738–27744.
- (19) Ren, L.; Yuan, P.; Su, H.; Malola, S.; Lin, S.; Tang, Z.; Teo, B. K.; Häkkinen, H.; Zheng, L.; Zheng, N. Bulky Surface Ligands Promote Surface Reactivities of $[Ag_{141}X_{12}(S-Adm)_{40}]^{3+}$ (X = Cl, Br, I) Nanoclusters: Models for Multiple-Twinned Nanoparticles. *J. Am. Chem. Soc.* **2017**, *139*, 13288–13291.
- (20) Hu, X.; Zheng, Y.; Zhou, J.; Fang, D.; Jiang, H.; Wang, X. Silver-Assisted Thiolate Ligand Exchange Induced Photoluminescent Boost of Gold Nanoclusters for Selective Imaging of Intracellular Glutathione. *Chem. Mater.* **2018**, *30*, 1947–1955.
- (21) Sakthivel, N. A.; Dass, A. Aromatic Thiolate-Protected Series of Gold Nanomolecules and a Contrary Structural Trend in Size Evolution. *Acc. Chem. Res.* **2018**, *51*, 1774–1783.
- (22) Nimmala, P. R.; Dass, A. Au₃₆(SPh)₂₃ Nanomolecules. *J. Am. Chem. Soc.* **2011**, 133, 9175–9177.
- (23) Zeng, C.; Chen, Y.; Das, A.; Jin, R. Transformation Chemistry of Gold Nanoclusters: From One Stable Size to Another. *J. Phys. Chem. Lett.* **2015**, *6*, 2976–2986.
- (24) Dass, A.; Jones, T. C.; Theivendran, S.; Sementa, L.; Fortunelli, A. Core Size Interconversions of $Au_{30}(S-tBu)_{18}$ and $Au_{36}(SPhX)_{24}$. *J. Phys. Chem. C* **2017**, *121*, 14914–14919.
- (25) Theivendran, S.; Dass, A. Synthesis of Aromatic Thiolate-Protected Gold Nanomolecules by Core Conversion: The Case of Au₃₆(SPh-tBu)₂₄. *Langmuir* **2017**, *33*, 7446–7451.
- (26) Nimmala, P. R.; Theivendran, S.; Barcaro, G.; Sementa, L.; Kumara, C.; Jupally, V. R.; Apra, E.; Stener, M.; Fortunelli, A.; Dass, A. Transformation of $Au_{144}(SCH_2CH_2Ph)_{60}$ to $Au_{133}(SPh\text{-}tBu)_{52}$ Nanomolecules: Theoretical and Experimental Study. *J. Phys. Chem. Lett.* **2015**, *6*, 2134–2139.
- (27) Zeng, C.; Chen, Y.; Kirschbaum, K.; Appavoo, K.; Sfeir, M. Y.; Jin, R. Structural Patterns at All Scales in a Nonmetallic Chiral Au₁₃₃(SR)₅₂ Nanoparticle. *Sci. Adv.* **2015**, *1*, No. e1500045.
- (28) Gan, Z.; Xia, N.; Wu, Z. Discovery, Mechanism, and Application of Antigalvanic Reaction. Acc. Chem. Res. 2018, 51, 2774–2783.

- (29) Wang, S.; Li, Q.; Kang, X.; Zhu, M. Customizing the Structure, Composition, and Properties of Alloy Nanoclusters by Metal Exchange. *Acc. Chem. Res.* **2018**, *51*, 2784–2792.
- (30) Yang, S.; Chai, J.; Song, Y.; Fan, J.; Chen, T.; Wang, S.; Yu, H.; Li, X.; Zhu, M. In Situ Two-Phase Ligand Exchange: A New Method for the Synthesis of Alloy Nanoclusters with Precise Atomic Structures. *J. Am. Chem. Soc.* **2017**, *139*, 5668–5671.
- (31) Fernando, A.; Aikens, C. M. Ligand Exchange Mechanism on Thiolate Monolayer Protected Au₂₅(SR)₁₈ Nanoclusters. *J. Phys. Chem. C* **2015**, *119*, 20179–20187.
- (32) Fernando, A.; Aikens, C. M. Deciphering the Ligand Exchange Process on Thiolate Monolayer Protected Au₃₈(SR)₂₄ Nanoclusters. *J. Phys. Chem. C* **2016**, *120*, 14948–14961.
- (33) Niihori, Y.; Kikuchi, Y.; Kato, A.; Matsuzaki, M.; Negishi, Y. Understanding Ligand-Exchange Reactions on Thiolate-Protected Gold Clusters by Probing Isomer Distributions Using Reversed-Phase High-Performance Liquid Chromatography. ACS Nano 2015, 9, 9347–9356.
- (34) Ishida, Y.; Narita, K.; Yonezawa, T.; Whetten, R. L. Fully Cationized Gold Clusters: Synthesis of $Au_{25}(SR^+)_{18}$. J. Phys. Chem. Lett. **2016**, 7, 3718–3722.
- (35) Meng, X.; Xu, Q.; Wang, S.; Zhu, M. Ligand-Exchange Synthesis of Selenophenolate-Capped Au₂₅ Nanoclusters. *Nanoscale* **2012**, *4*, 4161–4165.
- (36) Kang, X.; Chong, H.; Zhu, M. Au₂₅(SR)₁₈: The Captain of the Great Nanocluster Ship. *Nanoscale* **2018**, *10*, 10758–10834.
- (37) Higaki, T.; Liu, C.; Zeng, C.; Jin, R.; Chen, Y.; Rosi, N. L.; Jin, R. Controlling the Atomic Structure of Au₃₀ Nanoclusters by a Ligand-Based Strategy. *Angew. Chem., Int. Ed.* **2016**, *55*, 6694–6697.
- (38) Kurashige, W.; Yamaguchi, M.; Nobusada, K.; Negishi, Y. Ligand-Induced Stability of Gold Nanoclusters: Thiolate versus Selenolate. *J. Phys. Chem. Lett.* **2012**, *3*, 2649–2652.
- (39) Zhuang, S.; Liao, L.; Yuan, J.; Wang, C.; Zhao, Y.; Xia, N.; Gan, Z.; Gu, W.; Li, J.; Deng, H.; et al. Kernel Homology in Gold Nanoclusters. *Angew. Chem., Int. Ed.* **2018**, *57*, 15450–15454.
- (40) Tang, Q.; Hu, G.; Fung, V.; Jiang, D.-e. Insights into Interfaces, Stability, Electronic Properties, and Catalytic Activities of Atomically Precise Metal Nanoclusters from First Principles. *Acc. Chem. Res.* **2018**, *51*, 2793–2802.
- (41) Xu, W. W.; Zeng, X. C.; Gao, Y. Application of Electronic Counting Rules for Ligand-Protected Gold Nanoclusters. *Acc. Chem. Res.* **2018**, *51*, 2739–2747.
- (42) Shibu, E. S.; Muhammed, M. A. H.; Tsukuda, T.; Pradeep, T. Ligand Exchange of Au₂₅SG₁₈ Leading to Functionalized Gold Clusters: Spectroscopy, Kinetics, and Luminescence. *J. Phys. Chem. C* **2008**, *112*, 12168–12176.
- (43) Rambukwella, M.; Burrage, S.; Neubrander, M.; Baseggio, O.; Aprà, E.; Stener, M.; Fortunelli, A.; Dass, A. Au₃₈(SPh)₂₄: Au₃₈ Protected with Aromatic Thiolate Ligands. *J. Phys. Chem. Lett.* **2017**, *8*, 1530–1537.
- (44) Dong, H.; Liao, L.; Wu, Z. Two-Way Transformation Between Fcc- and Nonfcc-Structured Gold Nanoclusters. *J. Phys. Chem. Lett.* **2017**, *8*, 5338–5343.
- (45) Higaki, T.; Liu, C.; Chen, Y.; Zhao, S.; Zeng, C.; Jin, R.; Wang, S.; Rosi, N. L.; Jin, R. Oxidation-Induced Transformation of Eight-Electron Gold Nanoclusters: $[Au_{23}(SR)_{16}]^-$ to $[Au_{28}(SR)_{20}]^0$. J. Phys. Chem. Lett. **2017**, 8, 866–870.
- (46) Dainese, T.; Antonello, S.; Bogialli, S.; Fei, W.; Venzo, A.; Maran, F. Gold Fusion: From Au₂₅(SR)₁₈ to Au₃₈(SR)₂₄, the Most Unexpected Transformation of a Very Stable Nanocluster. *ACS Nano* **2018**, *12*, 7057–7066.
- (47) Du, W.; Jin, S.; Xiong, L.; Chen, M.; Zhang, J.; Zou, X.; Pei, Y.; Wang, S.; Zhu, M. $Ag_{50}(Dppm)_6(SR)_{30}$ and Its Homologue $Au_xAg_{50-x}(Dppm)_6(SR)_{30}$ Alloy Nanocluster: Seeded Growth, Structure Determination, and Differences in Properties. *J. Am. Chem. Soc.* **2017**, *139*, 1618–1624.
- (48) Nimmala, P. R.; Dass, A. Au₉₉(SPh)₄₂ Nanomolecules: Aromatic Thiolate Ligand Induced Conversion of Au₁₄₄(SCH₂CH₂Ph)₆₀. J. Am. Chem. Soc. **2014**, 136, 17016–17023.

- (49) Higaki, T.; Liu, C.; Zhou, M.; Luo, T.-Y.; Rosi, N. L.; Jin, R. Tailoring the Structure of 58-Electron Gold Nanoclusters: Au₁₀₃S₂(S-Nap)₄₁ and Its Implications. *J. Am. Chem. Soc.* **2017**, *139*, 9994–10001.
- (50) Rambukwella, M.; Sementa, L.; Barcaro, G.; Fortunelli, A.; Dass, A. Organosoluble Au₁₀₂(SPh)₄₄ Nanomolecules: Synthesis, Isolation, Compositional Assignment, Core Conversion, Optical Spectroscopy, Electrochemistry, and Theoretical Analysis. *J. Phys. Chem. C* 2015, *119*, 25077–25084.
- (51) Sakthivel, N. A.; Stener, M.; Sementa, L.; Fortunelli, A.; Ramakrishna, G.; Dass, A. Au₂₇₉(SR)₈₄: The Smallest Gold Thiolate Nanocrystal That Is Metallic and the Birth of Plasmon. *J. Phys. Chem. Lett.* **2018**, *9*, 1295–1300.
- (52) Higaki, T.; Zhou, M.; Lambright, K. J.; Kirschbaum, K.; Sfeir, M. Y.; Jin, R. Sharp Transition from Nonmetallic Au₂₄₆ to Metallic Au₂₇₉ with Nascent Surface Plasmon Resonance. *J. Am. Chem. Soc.* **2018**, *140*, 5691–5695.
- (53) Sumner, L.; Sakthivel, N. A.; Schrock, H.; Artyushkova, K.; Dass, A.; Chakraborty, S. Electrocatalytic Oxygen Reduction Activities of Thiol-Protected Nanomolecules Ranging in Size from Au₂₈(SR)₂₀ to Au₂₇₉(SR)₈₄. *J. Phys. Chem. C* **2018**, *122*, 24809–24817.
- (54) Negishi, Y.; Nakazaki, T.; Malola, S.; Takano, S.; Niihori, Y.; Kurashige, W.; Yamazoe, S.; Tsukuda, T.; Häkkinen, H. A Critical Size for Emergence of Nonbulk Electronic and Geometric Structures in Dodecanethiolate-Protected Au Clusters. J. Am. Chem. Soc. 2015, 137, 1206–1212.
- (55) Kwak, K.; Thanthirige, V. D.; Pyo, K.; Lee, D.; Ramakrishna, G. Energy Gap Law for Exciton Dynamics in Gold Cluster Molecules. *J. Phys. Chem. Lett.* **2017**, *8*, 4898–4905.
- (56) Lopez-Acevedo, O.; Akola, J.; Whetten, R. L.; Grönbeck, H.; Häkkinen, H. Structure and Bonding in the Ubiquitous Icosahedral Metallic Gold Cluster Au₁₄₄(SR)₆₀. *J. Phys. Chem. C* **2009**, *113*, 5035–5038
- (57) Lei, Z.; Li, J.-J.; Wan, X.-K.; Zhang, W.-H.; Wang, Q.-M. Isolation and Total Structure Determination of an All-Alkynyl-Protected Gold Nanocluster Au₁₄₄. Angew. Chem., Int. Ed. **2018**, 57, 8639—8643.
- (58) Yan, N.; Xia, N.; Liao, L.; Zhu, M.; Jin, F.; Jin, R.; Wu, Z. Unraveling the Long-Pursued Au₁₄₄ Structure by X-Ray Crystallography. *Sci. Adv.* **2018**, *4*, No. eaat7259.
- (59) Dass, A.; Theivendran, S.; Nimmala, P. R.; Kumara, C.; Jupally, V. R.; Fortunelli, A.; Sementa, L.; Barcaro, G.; Zuo, X.; Noll, B. C. Au₁₃₃(SPh-tBu)₅₂ Nanomolecules: X-ray Crystallography, Optical, Electrochemical, and Theoretical Analysis. *J. Am. Chem. Soc.* **2015**, 137, 4610–4613.
- (60) Yang, H.; Wang, Y.; Chen, X.; Zhao, X.; Gu, L.; Huang, H.; Yan, J.; Xu, C.; Li, G.; Wu, J.; et al. Plasmonic Twinned Silver Nanoparticles with Molecular Precision. *Nat. Commun.* **2016**, *7*, 12809.
- (61) Zeng, C.; Li, T.; Das, A.; Rosi, N. L.; Jin, R. Chiral Structure of Thiolate-Protected 28-Gold-Atom Nanocluster Determined by X-ray Crystallography. *J. Am. Chem. Soc.* **2013**, *135*, 10011–10013.
- (62) Zeng, C.; Liu, C.; Pei, Y.; Jin, R. Thiol Ligand-Induced Transformation of $Au_{38}(SC_2H_4Ph)_{24}$ to $Au_{36}(SPh\text{-t-Bu})_{24}$. ACS Nano 2013, 7, 6138–6145.
- (63) Kumara, C.; Dass, A. Au₃₂₉(SR)₈₄ Nanomolecules: Compositional Assignment of the 76.3 kDa Plasmonic Faradaurates. *Anal. Chem.* **2014**, *86*, 4227–4232.
- (64) Qian, H.; Zhu, Y.; Jin, R. Atomically precise gold nanocrystal molecules with surface plasmon resonance. *Proc. Natl. Acad. Sci. U.S.A.* **2012**, *109*, 696–700.
- (65) Zhou, M.; Zeng, C.; Chen, Y.; Zhao, S.; Sfeir, M. Y.; Zhu, M.; Jin, R. Evolution from the Plasmon to Exciton State in Ligand-Protected Atomically Precise Gold Nanoparticles. *Nat. Commun.* **2016**, *7*, 13240.
- (66) Kumara, C.; Zuo, X.; Ilavsky, J.; Cullen, D.; Dass, A. Atomic Structure of Au₃₂₉(SR)₈₄ Faradaurate Plasmonic Nanomolecules. *J. Phys. Chem. C* **2015**, *119*, 11260–11266.